IEEE Access
Multidisciplinary | Rapid Review | Open Access Journal

Received 10 July 2024, accepted 3 August 2024, date of publication 12 August 2024, date of current version 22 August 2024.

Digital Object Identifier 10.1109/ACCESS.2024.3442532

RESEARCH ARTICLE

A Resonant-Cavity Antenna With High-Gain and Wide Bandwidth With an All-Dielectric 3D-Printed Superstrate

CRISTINA PONTI[1], (Member, IEEE), SILVIO CECCUZZI[2], PAOLO BACCARELLI[1], (Member, IEEE), AND GIUSEPPE SCHETTINI[1], (Senior Member, IEEE)

[1]Department of Industrial, Electronic and Mechanical Engineering, Roma Tre University, 00146 Rome, Italy
[2]Nuclear Department, ENEA, 00044 Frascati, Italy

Corresponding author: Cristina Ponti (cristina.ponti@uniroma3.it)

This work was supported in part by Italian Ministry for Education, University, and Research through the Project PRIN2017 "Quick, Reliable, Cost Effective Methodology for DIagnostics of Conformal Antennas (DI-CA)," under Grant 20177C3WRM_003.

ABSTRACT The 3D-printing of dielectric superstrates of Resonant Cavity Antennas has advantages of fast prototyping and flexibility in the realization of customized layouts. In this work, the low dielectric permittivity of test filaments is experimentally measured for their use in superstrates of Resonant Cavity Antennas. A suitable combination of thickness, side extension and permittivity of the superstrate can enhance the antenna gain of the primary source over a broad frequency interval. With non-periodic and perforated layouts, instead, the radiative properties can be improved in terms of reductions of the Side-Lobe Level. The use of an all-dielectric superstrate in the design of an RCA is presented, demonstrating the possibility of obtaining a broadband gain enhancement with a single dielectric layer of low permittivity.

INDEX TERMS 3D printing, additive manufacturing, electromagnetic-band gap (EBG), high gain, resonant-cavity antenna (RCA).

I. INTRODUCTION

Additive Manufacturing (AM) through Fusion Deposition Modeling (FDM) is a fast-prototyping technique with significant advantages in the fabrication of antenna parts [1]. Thanks to AM, complex 3D layouts can be shaped with a flexible and low-cost approach, compared to traditional machining techniques, leading to quick validation of antenna designs. An interesting example of application is the realization of all-dielectric artificial materials employed as superstrates of Resonant Cavity Antennas (RCAs) [2]. In the literature, these antennas are also known as Electromagnetic Band-Gap Resonator Antennas (ERAs), being the superstrate realized in a periodic form, as an Electromagnetic Band-Gap (EBG) material [3], or as Fabry-Perot Cavity Antennas [4], [5], [6], [7], [8]. In an RCA, the superstrate is a partially reflecting surface, placed at a resonating distance from a low-gain antenna backed by a ground plane, to enhance the gain of the primary source through a cavity layout. Therefore, a traditional RCA, implemented with a superstrate having a periodical layout, is extremely narrow-bandwidth, with a fractional bandwidth of 3%-4%. To increase the bandwidth of an RCA, designs of broadband superstrates implemented through non-periodic realizations have been developed, considering either printed dielectric layers or fully dielectric superstrates. A wideband response, for example, can be achieved through ultrathin printed layers [9], [10], assembled in multilayer behaving as partially reflective surface with positive phase gradient [11]. Alternatively, broadband multilayers have been proposed in the form of one-dimensional (1D) Electromagnetic Band-Gap (EBG) materials alternating in a non-periodic way dielectric slabs of different thickness and permittivity, in order to enlarge the unit transmission within the EBG stop band [12], [13]. The use of dielectrics in the realization of

The associate editor coordinating the review of this manuscript and approving it for publication was Ladislau Matekovits.

antenna superstrates has advantages over combined metallic/dielectric realizations, due to the low losses, paving the way to applications from millimeter waves to THz frequency ranges. Alternative realizations of dielectric broadband superstrates have been explored in the form of a 3D-printed single dielectric layer with a stepped profile, as in [14] and [15]. Otherwise, in [2], [14], and [16] the broadband response is provided by a circular dielectric layer of uniform thickness having a stepped permittivity, achieved through a non-uniform radial filling of the printing material. In recent advancements of RCAs, a beam-stearing of the field from the primary source is performed, through the assembling of fully-dielectric 3D-printed non-uniformly perforated layers [17], [18].

As to the filament material used in the superstrate realization, both low-permittivity filaments [19], high-permittivity ones [15], and metal-painted dielectrics [20] have been proposed. The use of low-permittivity plastic filaments, as the Polylactic Acid (PLA) and the Acrylonitrile Butadiene Styrene (ABS) materials, has advantages in the ease of the fabrication process and simplicity of the printing facility, while still demonstrating the possibility of enhancing the antenna gain also in broadband layouts [2], [16]. However, when broadband RCAs are considered, the superstrate has a small in-plane aperture, that leads to strong edge diffraction and, consequently, to limitations in the SLL. A broadband superstrate, combining the non-uniform 1D layout to a tapered in-plane realization of the layers in the form of grids, is presented in [21], and has demonstrated significant reduction of the SLL.

In this work, the use of a low permittivity filament is proposed for the superstrate of an RCA realized as a single layer, achieving a much larger bandwidth compared to a non-periodic multilayer using slabs of identical values of the dielectric permittivity [22], [23]. Furthermore, the single-layer realization of the superstrate has the advantage of making more practical the assembling of the superstrate to the primary source compared to a multilayer realization, while reducing: 1) errors in the spacing of the slabs; 2) warping of thinner slabs; 3) diffraction by the mounting structure, with effects on the radiative properties. Preliminarily, low-permittivity filaments have been measured with a Vector Network Analyzer to select the printing filament of the superstrate. The superstrate is proposed in the form of a single thick layer for a broadband gain-enhancement of the field radiated by a rectangular waveguide. In the final layout, the superstrate is realized as a perforated layer of non-uniform holes, which reduces the SLL and provides a general improvement to the gain, compared to a uniform realization.

In Section II, the results relevant to the measurement of different filaments of printing materials are presented. In Section III, the RCA has been proposed with a single layer superstrate of a low permittivity. In Section IV, experimental results are reported.

II. MEASUREMENTS ON 3D PRINTING MATERIALS

Four different materials of 3D-printing filaments have been printed in test samples for the characterization of the relevant dielectric permittivity through a Keysight Fieldfox Vector Network Analyzer (VNA). The considered filaments are polymers of low-permittivity and are the following: Acrylonitrile Butadiene Styrene (ABS), Acrylonitrile Styrene Acrylate (ASA), Polylactic Acid (PLA), and Thermoplastic Polyurethane (TPU). These filaments have been printed with the Ultimaker S5 3D-printer in the form of parallelepiped samples of length 22.86 mm, height 10.16 mm, and depth 9.63 mm, which fits the standard internal size of the WR90 sample holder used in X band (8.2 GHz – 12.4 GHz) rectangular waveguide calibration kit of the Fieldfox Keysight VNA. A picture of the printed samples enclosed in the X-band sample holder of the calibration kit is reported in Fig. 1.

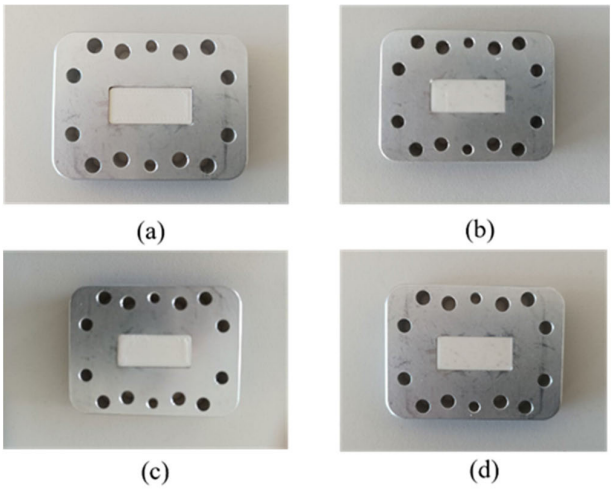

FIGURE 1. 3D-printed samples of length 22.86 mm, height 10.16 mm, and depth 9.63 mm in the X-band rectangular waveguide sample holder of the filaments: a) ABS; b) ASA; c) PLA; d) TPU.

The real part of the relative permittivity ε_r' and the tanδ have been retrieved using three different inversion algorithms: the Polynomial Fit proposed in [24], the Reflection-Transmission algorithms by Nicholson-Ross [25], and the Transmission Epsilon Fast algorithm, a technique developed in the Keysight Material Measurement Suite [26]. The reconstructed permittivities in the X band of the different filaments, ABS, ASA, PLA, TPU are shown in Fig. 2, comparing the estimated values of ε_r' and the tanδ with the three algorithms. As shown, the most stable results are obtained with the Polynomial Fit algorithm, that has been proposed for permittivity measurements of materials in transmission-line sample holder. Finally, results of the permittivity of the four filaments versus frequency, obtained with the Polynomial Fit, are compared in Fig. 3 and in Table 1, where the numerical values at the frequency of 12 GHz are reported. Results show that ABS, PLA and TPU have comparable ε_r' of about 2.6, and the lowest losses in ABS.

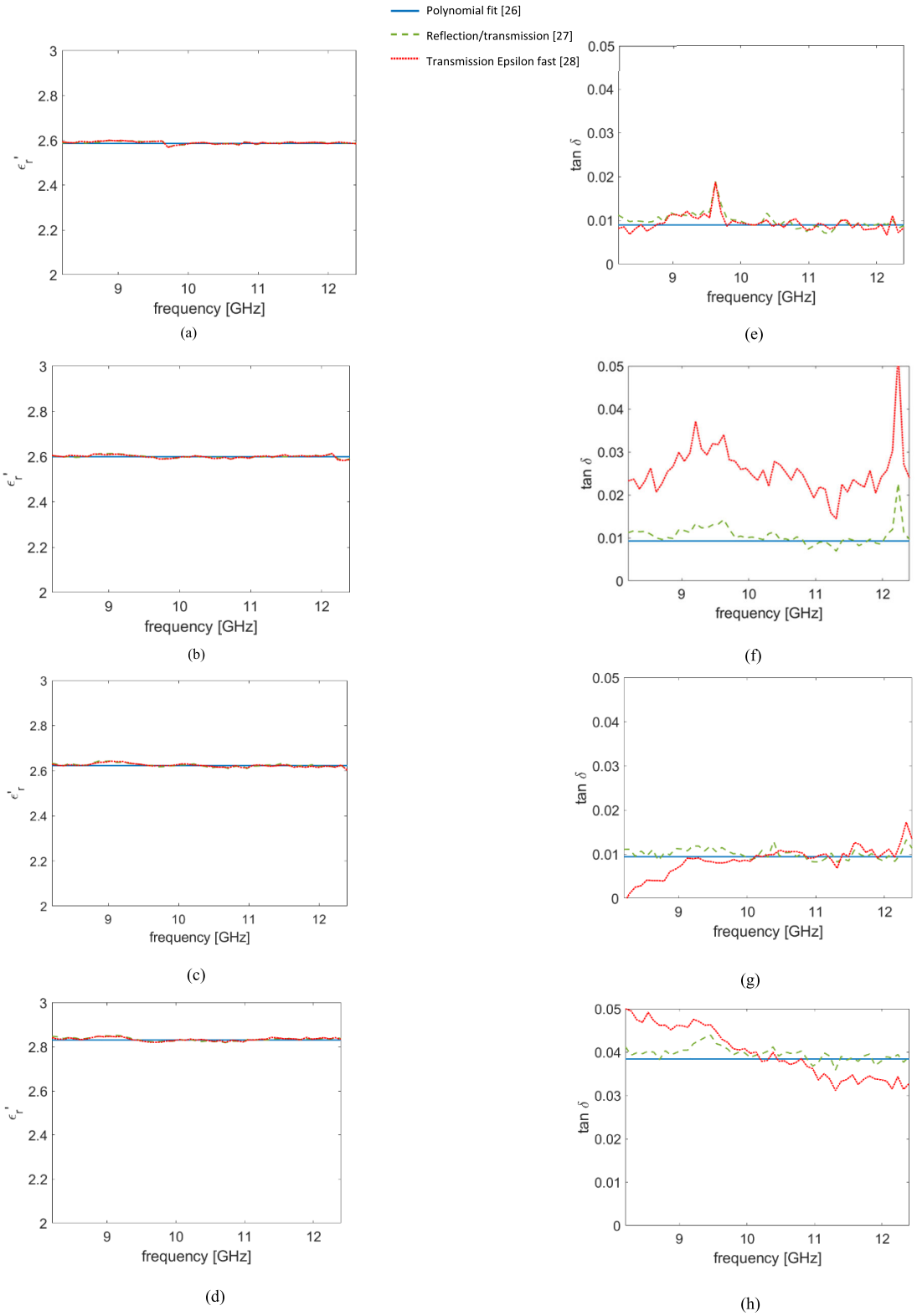

FIGURE 2. Retrieved permittivity from the X-band measurements on the samples in Fig. 1, comparing the reconstructions with Polynomial Fit [24], the Reflection-Transmission by Nicholson-Ross [25], and Transmission Epsilon Fast algorithm [26]: a) permittivity ε_r' of ABS; b) tanδ of ABS; c) permittivity ε_r' of ASA d) tanδ of ASA; e) permittivity ε_r' of PLA; f) tanδ of PLA; g) permittivity ε_r' of TPU; h) tanδ of TPU.

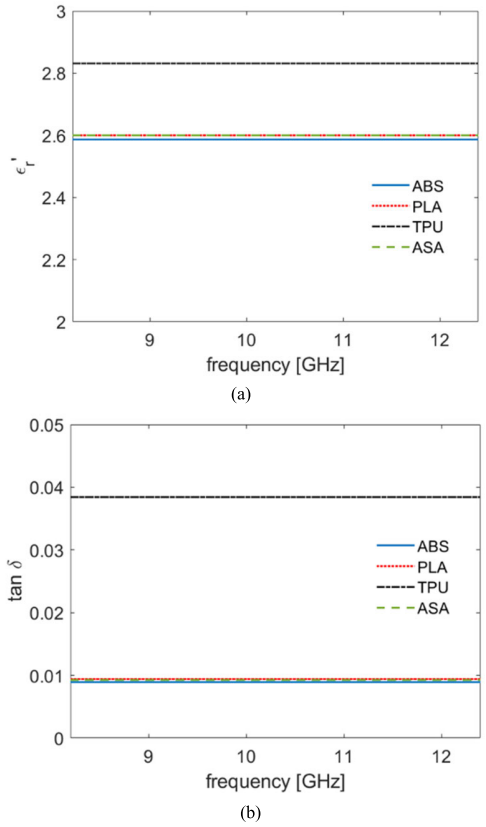

FIGURE 3. Dielectric permittivity versus frequency of the samples of ABS, ASA, PLA and TPU of Fig. 1 determined from the measurements with the Polynomial Fit [24]: a) relative permittivity ε'_r; b) tan δ.

TABLE 1. Measured values of dielectric permittivity on 3D-printed samples at 12 GHz with the polynomial fit [24].

Material	ε_r	tanδ
ABS	2.58	0.009
ASA	2.59	0.011
PLA	2.62	0.011
TPU	2.83	0.039

As to TPU, it has the highest ε'_r, of about 2.8, but the high losses, with tan$\delta = 0.039$, would reduce the radiation efficiency when used as an antenna superstrate, especially if realized in the form of thick dielectric layer.

About the use of ABS, ASA, and PLA, i.e., the filaments with the lowest losses, in the realization of an RCA superstrate, mechanical properties can be also considered [27], [28], [29]. ABS and ASA filaments have better properties in terms of warping, compared to PLA, which makes them more suitable for the realization of thin parts. As to ASA, it has a very good surface finishing, with smooth printing, and has properties suitable for its use in outdoor environments, for its UV/weather resistance.

III. THE RESONANT-CAVITY ANTENNA

The 3D-printing materials characterized in Section II have been checked as superstrates of an RCA, in which the primary source is a truncated rectangular waveguide surrounded by a metallic plate (perfectly electric conductor, PEC), as shown in the cross-section sketched as schematic view in Fig. 4. Basically, in the RCA two resonating media are assembled, a vacuum-filled region, of vertical length h, followed by a dielectric-filled parallelepipedal volume, of height t and side L in both x- and y-directions. The combination of the two cavity lengths h and t is such to provide a broadband interaction between the primary source and the resonating regions above, approximatively in the frequency range [10 – 18 GHz]. In the designed RCA, the length of the air region is $h = \lambda_0/2$, and the superstrate has side $L = 1.35\lambda_0$, and height $t = 0.83\lambda_0$, where λ_0 corresponds to the lowest operating frequency of 10 GHz. The sizes of h, L, and t have been obtained from a parametric study aiming at a maximization of the bandwidth. For an average dielectric permittivity $\varepsilon_r = 2.6$ of the superstrate material, the selected values L and t allow for the resonance of frequencies up to 18 GHz of higher order modes of the cavity. In the design, the RCA has been simulated considering a truncated rectangular waveguide with standard size in the X band. As to the permittivity of the superstrate, the estimated value of the ABS in Table 1 has been used. Furthermore, in the simulated layout, the side structure to assemble to the printed layer to the metallic plate is also included, as shown in Fig. 6(a). Indeed, as observed in [21], due to the small footprint area, the radiative properties of an RCA are affected by the mounting structure, made by side extensions and screws, which reduce the nominal gain simulated with a suspended superstrate. Therefore, the mounting structure must be included in the numerical model for a correct prediction of the gain of the fabricated prototype. However, in this model, which uses a very thick superstate, the diffraction is smaller, compared to the multilayer realization proposed in [21]. The side extensions, indeed, are placed at the bottom of the superstrate and the radiation pattern is less affected. The RCA layout of Fig. 5(a) is proposed also using a perforated superstrate, shown in Fig. 5(b), in which the concept of a tapered grid, developed for a reduced side diffraction and thus lower SLL, is implemented [21]. The superstrate in Fig. 5(b) is shown in its in-plane realization in Fig. 6(b), it is made by non-uniformly spaced holes of non-uniform size, enlarging from the center to the edge of the structure, as shown in the top view of Fig. 6(b). The design parameters of the tapered grid are d_i and w_i (i = 1,2,3), selected applying a sinusoidal tapering law [30], which determines a reduction in reflectivity from the center to the edge of the structure. From a parametric study, the values $d_1 = 3.35 =$ mm, $d_2 = 6$ mm, $w_1 = 8$ mm, $w_2 = 5.3$ mm, $w_3 = 2.7$ mm have been selected.

The simulated gain versus frequency for the antennas in Fig. 5(a) and 5(b) are compared in Fig. 7 and Table 2. With both the uniform and grid superstrate, a broadband response

is observed, in which the gain of the primary source is enhanced.

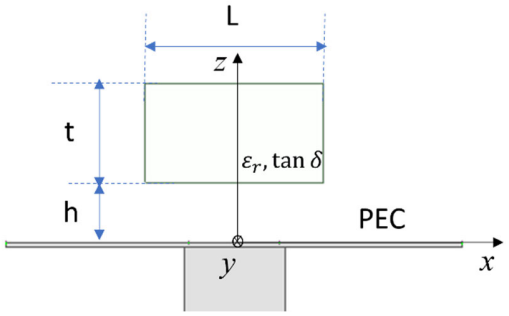

FIGURE 4. Cross-sectional view of the RCA.

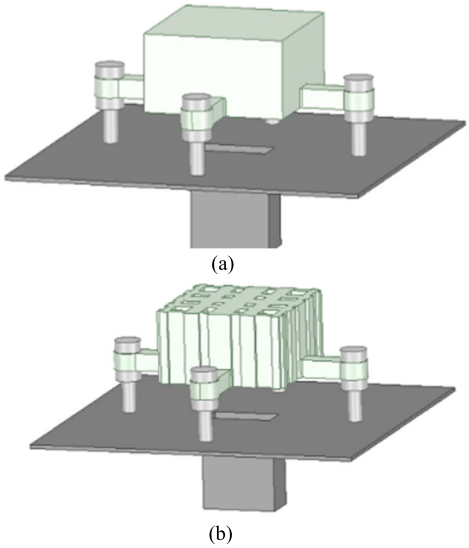

FIGURE 5. Perspective view of the RCA in Fig. 2 with the different superstrates: a) homogeneous superstrate; b) grid superstrate.

The truncated rectangular waveguide has an increasing gain from 5.5 dB to 10 dB in the frequency range [10 – 18 GHz]. The RCA with uniform superstrate shows a gain enhancement over the antenna without superstrate of about 9 dB at the lowest edge of the frequency interval. As the frequency is increased, instead, the gain enhancement is smaller, with a drop at 15 GHz and 17 GHz. As to the RCA with grid superstrate, instead, the gain keeps a uniform enhancement of 10 dB over the whole frequency interval, with a drop only in the highest edge, close to 18 GHz. In the RCA with uniform superstrate case, the peak gain is 16.4 dB, at the frequency of 10.6 GHz with 3 dB gain bandwidth spanning in the frequency interval [10 – 18 GHz], corresponding to a fractional bandwidth 57%. As to the RCA with grid superstate, instead, a peak gain of 18.4 dB is achieved at the frequency of 16.8 GHz, with a 3 dB gain fractional bandwidth of 56% in the interval [10.2 – 18 GHz]. At frequencies higher 18 GHz, the gain is still higher than the 3 dB value. Therefore, differently from what observed with uniform superstrate, with grid superstrate the bandwidth is larger than 56% if frequencies beyond the 18 GHz upper limit are considered. The values of the gain, without superstrate, with uniform superstrate and with grid superstrate are finally compared in Table 2, at frequencies sampled in the interval [10 – 18 GHz].

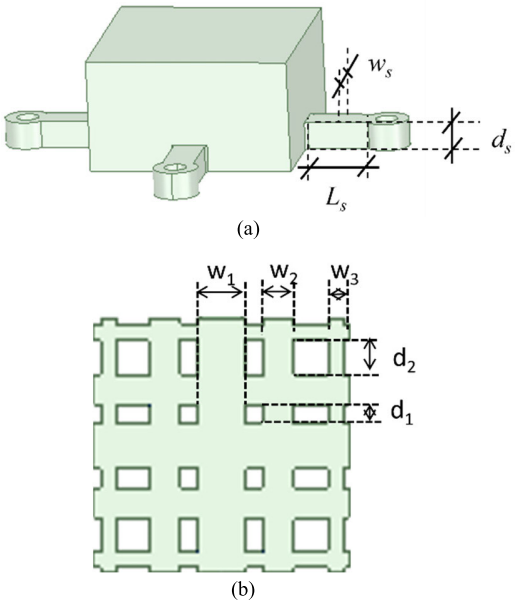

FIGURE 6. Details of the RCA superstrates in Fig. 5: a) side extensions used both in the uniform and grid superstrate, with size $L_s = 15.75$ mm, $w_s = 7$ mm, $d_s = 6$ mm; b) grid layout of the superstrate in Fig. 5(b), with: $d_1 = 3.35$ mm, $d_2 = 6$ mm, $w_1 = 8$ mm, $w_2 = 5.3$ mm, $w_3 = 2.7$ mm.

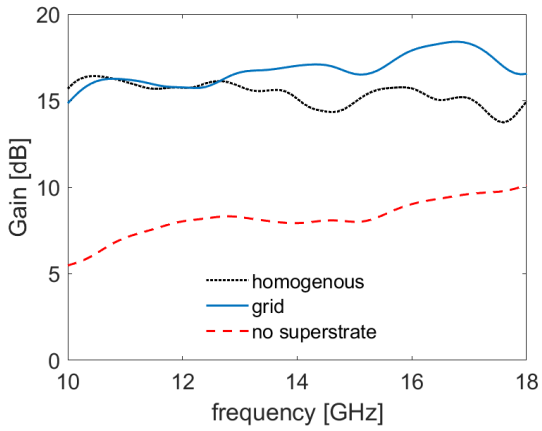

FIGURE 7. Gain versus frequency for the RCAs in Fig. 5, with homogeneous ABS superstrate (Fig. 5(a)) and grid ABS superstrate (Fig. 5(b)), compared to the gain of the antenna without superstrate.

The effective interaction of the RCA with the grid superstrate is confirmed in the far-field plots in Fig. 8, in which the normalized gain to the maximum value of the two antennas of Fig. 5 is reported, sampled at four frequencies: 10 GHz, 12 GHz, 14 GHz, 16 GHz. It can be appreciated that, especially in the H plane, a lower SLL is achieved with the grid layout. The different SLL is highlighted in the shaded-yellow

region. This general result is confirmed by the plot of the SLL as a function of frequency in the H- and E-planes, for the two different superstrates, reported in Fig. 9. For the grid superstrate, in the H-plane a SLL reduction larger than 10 dB is observed, compared to the homogeneous realization. Results for this antenna are summarized in Table 3.

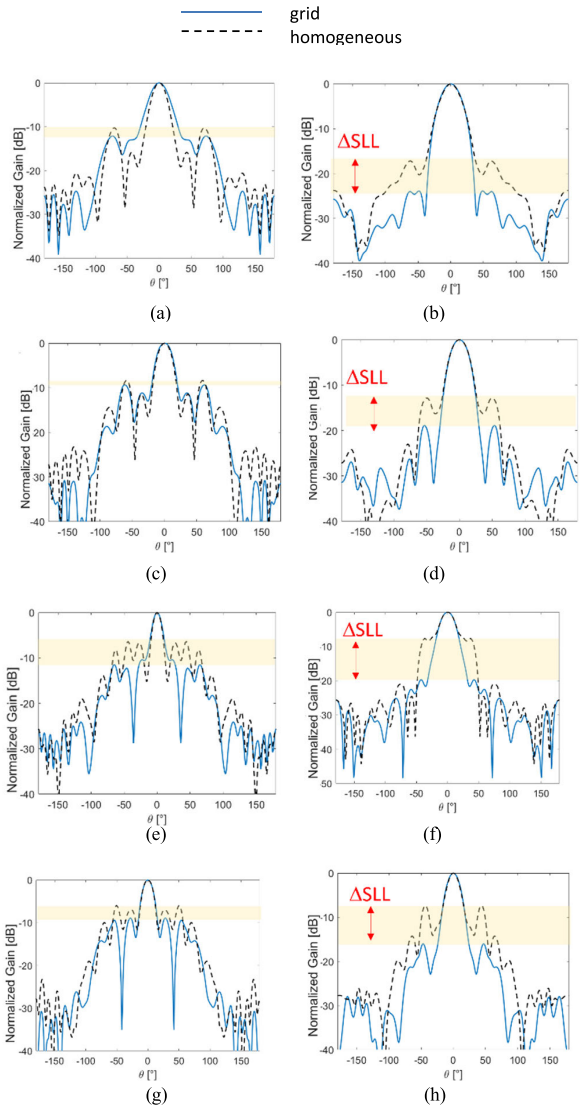

FIGURE 8. Far-fields plot of the normalized gain of the RCA with uniform superstrate (dotted line) and grid superstrate (solid line) in Fig. 5: a) 10 GHz, E-plane; (b) 10 GHz, H-plane; (c) 12 GHz, E-plane; (d) 12 GHz, H-plane; (e) 14 GHz, E-plane; (f) 14 GHz, H-plane; (e) 16 GHz, E-plane; (f) 16 GHz, H-plane.

Finally, to check the choice of the ABS superstrate in the RCA design, the antenna layout with grid superstrate in Fig. 5(b) is simulated also with the other printing filaments considered in Section II. Simulated results in Fig. 10 show that TPU, presenting a $\tan\delta = 0.039$, provides the highest difference between Gain and Directivity, i.e., of the radiation efficiency. Data of Gain and Directivity for the superstrates with the different materials are compared in Table 4.

TABLE 2. Data on the simulated Gain [dB] in Fig. 7 without superstrate, with homogeneous superstrate, and with grid superstrate.

Frequency [GHz]	No superstrate	homogeneous	grid
10	5.5	15.7	14.8
11	7.1	16.2	16.2
12	8.0	15.8	15.8
13	8.3	15.8	16.6
14	7.9	15.1	17.0
15	8.0	14.9	16.5
16	9.0	15.7	17.9
17	9.6	15.1	18.3
18	10.0	15.0	16.5

TABLE 3. Data on the maximum gain, bandwidth and SLL of the RCA with homogeneous superstrate, and with grid superstrate (Fig. 5).

RCA superstrate	Homogeneous	Grid
Peak Gain [dB]	16.4	18.4
Bandwidth [%]	57	> 56
SLL E-plane [dB]	-10.3	-11.9
SLL H-plane [dB]	-17.3	-27.1

TABLE 4. Gain and directivity in dB for the RCAs with grid superstrate simulated in Fig. 10.

RCA material	12 GHz		14 GHz		16 GHz	
	Gain	Dir.	Gain	Dir.	Gain	Dir.
ABS	15.77	15.85	17.02	17.08	17.91	19.11
ASA	15.74	15.85	17.07	17.98	17.34	18.00
PLA	15.69	15.84	16.86	17.00	18.16	18.35
TPU	15.60	15.32	16.31	16.75	17.31	18.19

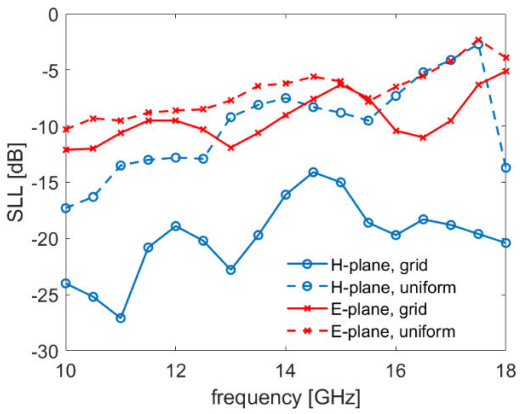

FIGURE 9. Side-Lobe Level versus frequency in the E and H plane for the RCA with grid superstrate (solid lines) and homogeneous superstrate (dotted line).

IV. EXPERIMENTAL RESULTS

The final realization of an RCA prototype in Fig. 5(b) is shown in Fig. 11. The superstrate has been 3D-printed

in the form of a grid with side extension as described in Fig. 6(a)-(b), using the ABS filament experimentally characterized in Section II. The printed superstrate has been assembled to an X-band rectangular waveguide as antenna source, surrounded by an aluminum plate: a top and bottom view of the ABS superstrate is shown in Fig. 11(b) and 11(c), respectively. In the experimental results, as shown, the propagation in the rectangular waveguide turns out to be multimodal due to the excitation of higher-order modes, in particular the TE_{01}, having cut-off frequency at 14.7 GHz, and the degenerate modes TE_{11} – TM_{11}, with cut-off frequency of 16.1 GHz The simulated and measured Directivity versus frequency are compared in Fig. 12: we can observe an excellent agreement up to 16.1 GHz. The drop in the measured Directivity at frequencies higher than 16.1 GHz is due to the excitation of the modes TE_{11} – TM_{11}.

As to the return loss reported in Fig. 13, a disagreement between measured and simulated data appears for frequencies beyond 14.7 GHz, corresponding to the excitation of the TE_{01} mode. This can be related primarily to coaxial-to-N transition used to feed the primary source, which excites higher order modes in the rectangular waveguide. The plots of the far-field patterns of the normalized gain, comparing the measured gain to the simulated gain of the antenna, are reported in Fig. 14. They are relevant to the frequencies of 10 GHz, 12 GHz, and 14 GHz, which fall in the frequency interval of good coupling of the excitation field with monomodal field of the waveguide.

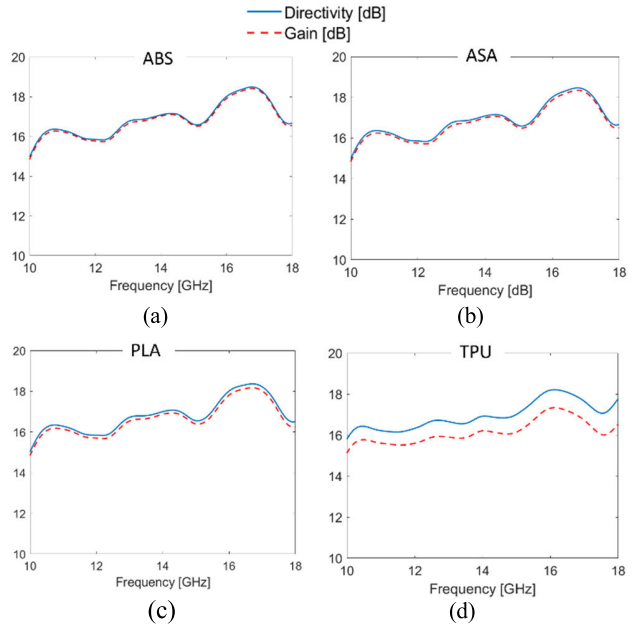

FIGURE 10. Directivity and Gain of the RCA with the grid superstrate in Fig. 5(b), with permittivity of: a) ABS; b) ASA; c) PLA; d) TPU.

In the same plots, the level of the cross-polarized component is shown. It can be observed that the radiation pattern confirms a very low SLL in the H plane in the measured

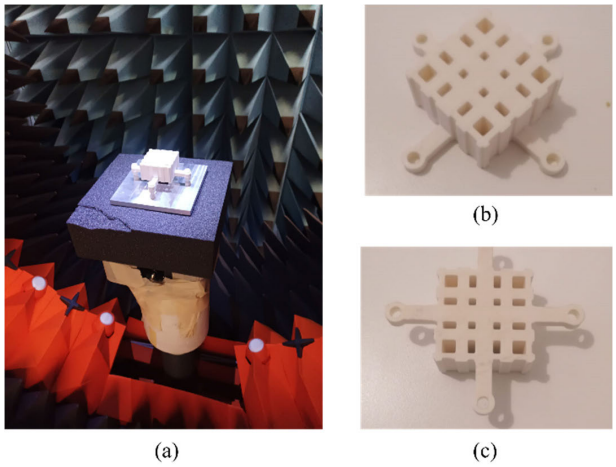

FIGURE 11. Photos of the fabricated antenna prototype: a) antenna prototype placed in the anechoic chamber; b) top view of the antenna superstrate; c) bottom view of the antenna superstrate.

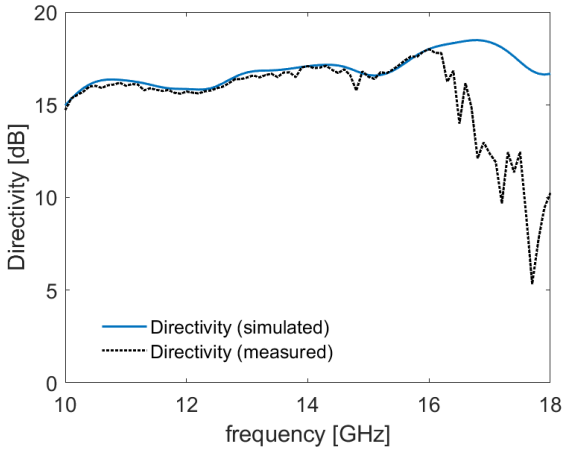

FIGURE 12. Directivity versus frequency of the RCA in Fig. 11, compared to measure results.

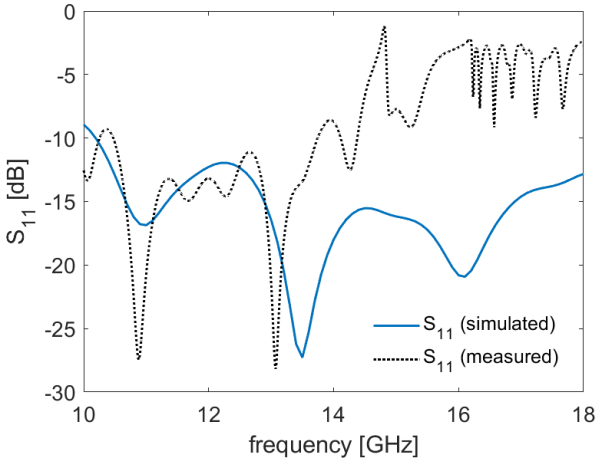

FIGURE 13. Magnitude of the reflection coefficient (dB) of the RCA of Fig. 11 compared to simulated results.

results. Furthermore, the agreement between measured and simulated data is very good. This is due to the preliminary

TABLE 5. Comparison of the performances of the new antenna with published broadband and High-Gain RCAs with dielectric superstrate.

	PRS type	f_0[GHz]	Height (λ_0)	Footprint (λ_0^2)	Peak Directivity [dB]	Bandwidth (%)	SLL E-plane [dB]	SLL H-plane [dB]
This work	Single layer	10	1.30	2.25	18.2	> 56	-11.9	-27.1
[21] Case A	multilayer	8.8	1.22	3.48	17.8	30	-9	-12
[21] Case B	multilayer	9.6	1.10	2.88	16.2	35	-15	-26
[2]	stepped permittivity gradient	10.7	0.97	2.86	16.05	49.65	-	below -12.7
[16]	staircase	10.75	0.9	5.3	20.7	56	-12	-21
[14]	staircase/multilayer	10.9	1.09	8.4	20.3	9.4	-	-17

characterization of the permittivity of the printing materials, but also to a design which has included the whole assembling structure, i.e., the side extension and the fixing screws and nuts, which strongly affect the final radiation in a small-size superstrate.

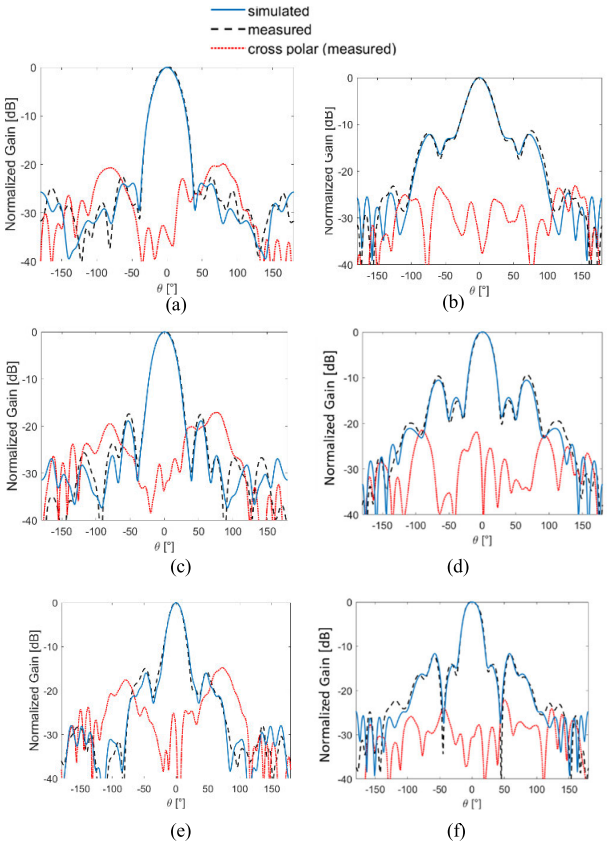

FIGURE 14. Far-field plots of normalized gain of the antenna of Fig. 11 (black dashed line), compared to simulated results (blue solid line), and measured cross-polarized component (red dotted line). (a) 10 GHz, E-plane. (b) 10 GHz, H-plane. (c) 12 GHz, E-plane. (d) 12 GHz, H-plane. (e) 14 GHz, E-plane. (f) 14 GHz, H-plane.

The values of peak measured gain, compared to the relevant simulated value, are reported in Table 6. The difference between the measured and simulated gain is of 1.2 dB at 10 GHz, and lower than 1 dB at 12 and 14 GHz. The difference is due to the K – to – N coaxial connector used in the anechoic chamber, which is not included in the calibration procedure.

TABLE 6. Data of PeaK Measured Gain and Peak Simulated Gain at the frequencies of Fig. 14.

Frequency [GHz]	10	12	14
Measured Gain [dB]	13.7	15.1	16.1
Simulated Gain [dB]	14.9	15.8	17.0

The properties of the presented antenna in terms of Peak Directivity, Bandwidth and SLL are compared in Table 5 to other RCAs with dielectric superstrate taken from the literature, in which the broadband superstrate is designed in the form of a multilayer [21], stepped permittivity gradient [2], staircase [16], and a combined staircase/multilayer realization [14], with their height and footprint area evaluated at the lowest operational frequency f_0. It can be appreciated that the antenna presented in this paper, although of slightly thicker height, has very good performances in terms of peak directivity and bandwidth, and shows the best results in terms of the SLL, especially in the H-plane.

V. CONCLUSION

The paper has shown the possibility of implementing an RCA with a superstrate which is a fully dielectric one of low permittivity. This choice is compatible with the properties of cheap and general-purpose printing filaments used in 3D printing with FDM technique. As to the realization of the RCA superstrate, a layout with a single layer has been proposed, in the form of a non-uniform perforated grid, which allows an easy assembling to the primary source while providing a broadband response and a gain enhancement. Measured data on the RCA with the superstrate made of ABS have been presented, which show very good agreement in the monomodal frequency interval of the source. Future works will regard the assembling of the superstrates to different realizations of the source, and the investigation of a thickness reduction of the superstrate with higher-permittivity dielectrics used in the 3D printing.

ACKNOWLEDGMENT

The authors thank the Microwave Vision Group for their support in the antenna measurements, using their Starlab 50 GHz Spherical Near Field Measurement System.

REFERENCES

[1] T. Whittaker, S. Zhang, A. Powell, C. J. Stevens, J. Y. C. Vardaxoglou, and W. Whittow, "3D printing materials and techniques for antennas and metamaterials: A survey of the latest advances," *IEEE Antennas Propag. Mag.*, vol. 65, no. 3, pp. 10–20, Jun. 2023.

[2] T. Hayat, M. U. Afzal, F. Ahmed, S. Zhang, K. P. Esselle, and Y. Vardaxoglou, "Low-cost ultrawideband high-gain compact resonant cavity antenna," *IEEE Antennas Wireless Propag. Lett.*, vol. 19, pp. 1271–1275, 2020.

[3] S. Yarga, K. Sertel, and J. L. Volakis, "Degenerate band edge crystals for directive antennas," *IEEE Trans. Antennas Propag.*, vol. 56, no. 1, pp. 119–126, Jan. 2008.

[4] S. Ceccuzzi, L. Pajewski, C. Ponti, and G. Schettini, "Directive EBG antennas: A comparison between two different radiating mechanisms," *IEEE Trans. Antennas Propag.*, vol. 62, no. 10, pp. 5420–5424, Oct. 2014.

[5] A. R. Weily, L. Horvath, K. P. Esselle, B. C. Sanders, and T. S. Bird, "A planar resonator antenna based on a woodpile EBG material," *IEEE Trans. Antennas Propag.*, vol. 53, no. 1, pp. 216–223, Jan. 2005.

[6] Y. J. Lee, J. Yeo, R. Mittra, and W. S. Park, "Application of electromagnetic bandgap (EBG) superstrates with controllable defects for a class of patch antennas as spatial angular filters," *IEEE Trans. Antennas Propag.*, vol. 53, no. 1, pp. 224–235, Jan. 2005.

[7] F. Frezza, L. Pajewski, E. Piuzzi, C. Ponti, and G. Schettini, "Analysis and experimental characterization of an alumina woodpile-covered planar antenna," in *Proc. 40th Eur. Microw. Conf.*, Sep. 2010, pp. 200–203.

[8] Y. Lee, X. Lu, Y. Hao, S. Yang, J. R. G. Evans, and C. G. Parini, "Low-profile directive millimeter-wave antennas using free-formed three-dimensional (3-D) electromagnetic bandgap structures," *IEEE Trans. Antennas Propag.*, vol. 57, no. 10, pp. 2893–2903, Oct. 2009.

[9] Y. Ge, K. P. Esselle, and T. S. Bird, "The use of simple thin partially reflective surfaces with positive reflection phase gradients to design wideband, low-profile EBG resonator antennas," *IEEE Trans. Antennas Propag.*, vol. 60, no. 2, pp. 743–750, Feb. 2012.

[10] F. Anelli, A. M. Loconsole, V. Portosi, A. Annunziato, V. V. Francione, and F. Prudenzano, "A wideband flexible Fabry–Perot resonator antenna: Inkjet-printing on ultrathin PET layers," in *Proc. IEEE Conf. Antenna Meas. Appl. (CAMA)*, Genoa, Italy, Nov. 2023, pp. 972–976.

[11] D. Jackson and N. Alexopoulos, "Gain enhancement methods for printed circuit antennas," *IEEE Trans. Antennas Propag.*, vols. AP-33, no. 9, pp. 976–987, Sep. 1985.

[12] R. M. Hashmi, B. A. Zeb, and K. P. Esselle, "Wideband high-gain EBG resonator antennas with small footprints and all-dielectric superstructures," *IEEE Trans. Antennas Propag.*, vol. 62, no. 6, pp. 2970–2977, Jun. 2014.

[13] N. Wang, L. Talbi, Q. Zeng, and J. Xu, "Wideband Fabry–Perot resonator antenna with electrically thin dielectric superstrates," *IEEE Access*, vol. 6, pp. 14966–14973,2018.

[14] T. Hayat, M. U. Afzal, A. Lalbakhsh, and K. P. Esselle, "3-D-Printed phase-rectifying transparent superstrate for resonant-cavity antenna," *IEEE Antennas Wireless Propag. Lett.*, vol. 18, pp. 1400–1404, 2019.

[15] A. A. Baba, R. M. Hashmi, K. P. Esselle, and A. R. Weily, "Compact high-gain antenna with simple all-dielectric partially reflecting surface," *IEEE Trans. Antennas Propag.*, vol. 66, no. 8, pp. 4343–4348, Aug. 2018.

[16] A. A. Baba, R. M. Hashmi, and K. P. Esselle, "Achieving a large gain-bandwidth product from a compact antenna," *IEEE Trans. Antennas Propag.*, vol. 65, no. 7, pp. 3437–3446, Jul. 2017.

[17] T. Hayat, M. U. Afzal, F. Ahmed, S. Zhang, K. P. Esselle, and J. Vardaxoglou, "The use of a pair of 3D-printed near field superstructures to steer an antenna beam in elevation and azimuth," *IEEE Access*, vol. 9, pp. 153995–154010, 2021.

[18] A. A. Baba, R. M. Hashmi, M. Attygalle, K. P. Esselle, and D. Borg, "Ultrawideband beam steering at mm-wave frequency with planar dielectric phase transformers," *IEEE Trans. Antennas Propag.*, vol. 70, no. 3, pp. 1719–1728, Mar. 2022.

[19] T. Hayat, M. U. Afzal, A. Lalbakhsh, and K. P. Esselle, "Additively manufactured perforated superstrate to improve directive radiation characteristics of electromagnetic source," *IEEE Access*, vol. 7, pp. 153445–153452, 2019.

[20] S. Shrestha, S. M. Abbas, M. Asadnia, and K. P. Esselle, "Realization of three dimensional printed multi layer wide band prototype," *IEEE Access*, vol. 10, pp. 130944–130954, 2022.

[21] C. Ponti, P. Baccarelli, S. Ceccuzzi, and G. Schettini, "Tapered all-dielectric EBGs with 3-D additive manufacturing for high-gain resonant-cavity antennas," *IEEE Trans. Antennas Propag.*, vol. 69, no. 5, pp. 2473–2480, May 2021.

[22] C. Ponti, P. Baccarelli, S. Ceccuzzi, and G. Schettini, "3D-printed dielectric superstrates for broadband and high-gain antennas," in *Proc. Int. Conf. Electromagn. Adv. Appl. (ICEAA)*, Venice, Italy, Oct. 2023, pp. 313–315.

[23] C. Ponti, P. Baccarelli, S. Ceccuzzi, and G. Schettini, "3D printing materials for the superstrate of a resonant-cavity antenna," in *Proc. IEEE Conf. Antenna Meas. Appl. (CAMA)*, Genoa, Italy, Nov. 2023, pp. 802–803.

[24] P. G. Bartley and S. B. Begley, "A new technique for the determination of the complex permittivity and permeability of materials," in *IEEE Instrum. Meas. Technol. Conf. Proc.*, May 2010, pp. 54–57.

[25] A. M. Nicolson and G. F. Ross, "Measurement of the intrinsic properties of materials by time-domain techniques," *IEEE Trans. Instrum. Meas.*, vols. IM-19, no. 4, pp. 377–382, Nov. 1970.

[26] *N1500A Materials Measurement Suite, Keysight*. [Online]. https://www.keysight.com/us/en/product/N1500A/materials-measurement-suite.html

[27] *ABS Datasheet, 3DItaly*. [Online]. Available: https://www.3ditaly.it/datasheet/Filamenti/ABS-datashet-V1.pdf

[28] *ASA Datasheet, 3DItaly*. [Online]. Available: https://www.3ditaly.it/datasheet/Filamenti/ASA-datashet-V1.pdf

[29] *PLA Datasheet, 3DItaly*. [Online]. Available: https://www.3ditaly.it/datasheet/Filamenti/PLA-datashet-V2.pdf

[30] C. Ponti, S. Ceccuzzi, G. Schettini, and P. Baccarelli, "Tapered EBG superstrates for low-permittivity resonator antennas," in *Proc. IEEE Int. Symp. Antennas Propag. (APSURSI)*, Jun. 2016, pp. 345–346.

CRISTINA PONTI (Member, IEEE) received the Laurea and Laurea Magistralis degrees (cum laude) in electronic engineering from the "Sapienza" University of Rome, Rome, Italy, in 2004 and 2006, respectively, and the Ph.D. degree from Roma Tre University, Rome, in 2010. Since 2021, she has been a tenure-track Assistant Professor of electromagnetic fields at Roma Tre University. She has achieved the Italian qualification for the roles of an Associate Professor and a Full Professor of electromagnetic fields. Her research interests include electromagnetic analysis, scattering problems, buried-objects detection, ground-penetrating radar, through-the-wall radar, numerical methods, electromagnetics-bandgap and artificial materials, antennas, and microwave components for high-power applications. She is a member of the IEEE Antennas and Propagation, Microwave Theory and Technique and Women in Engineering Societies, the National Interuniversity Consortium for Telecommunications (CNIT), and Italian Society of Electromagnetics (SIEm). She was the Co-Convener of conference sessions on the theme of scattering and antennas and served in the technical program committees of international conferences. She is an Associate Editor of *IET Microwaves, Antennas and Propagation*.

SILVIO CECCUZZI was born in Rome, Italy, in 1983. He received the Laurea di Primo Livello and Laurea Specialistica (cum laude) degrees in electronic engineering and the Ph.D. degree in applied electronics from Rome Tre University, Rome, in 2005, 2008, and 2015, respectively. He did an Internship with Telespazio, Rome, and Thales Alenia Space, Rome, in 2009. He started a three-year scholarship on high-power RF systems across European Laboratories. In 2013, he joined as a Researcher with Italian Energy and Environment Agency (ENEA), Frascati, Italy, where he became responsible for the ion-cyclotron heating system of the Divertor Tokamak Test facility, in 2021. Since 2016, he has been a Visiting Researcher with Rome Tre University. He has authored or co-authored more than 150 works on technical reports, journals, and conference proceedings. His current research interests include EBG, microwave components, and nuclear fusion. He received the 2015 IEEE MTT-S Award of the Chapter Central and Southern Italy and the Sannino Award of the Italian meeting RiNEm, in 2012.

PAOLO BACCARELLI (Member, IEEE) received the Laurea degree in electronic engineering and the Ph.D. degree in applied electromagnetics from the ''La Sapienza'' University of Rome, in 1996 and 2000, respectively. In 1996, he joined the Department of Electronic Engineering, ''La Sapienza'' University of Rome, where he has been an Assistant Professor, since November 2010. From April 1999 to October 1999, he was a Visiting Researcher with the University of Houston, Houston, TX, USA. In 2017, he joined the Department of Engineering, University of ''Roma Tre'', Rome, where he was an Associate Professor, from July 2017 to October 2023. In 2017, he passed the National Scientific Qualification, and in 2023, he definitively achieved the role of a Full Professor in the sector of electromagnetic fields with the Department of Industrial, Electronic, and Mechanical Engineering, University of ''Roma Tre'', Rome. He has co-authored about 300 papers in international journals, conference proceedings, and book chapters. His research interests include the analysis and design of leaky-wave antennas and arrays, numerical methods for integral equations and periodic structures, propagation and radiation in anisotropic media, metamaterials, graphene, and electromagnetic band-gap structures. He has been a member of the TPCs of several international conferences. He was the Secretary of the EuMW 2009 and a member of the Local Organizing Committee of the XXXIV URSI GASS 2021.

GIUSEPPE SCHETTINI (Senior Member, IEEE) received the Laurea degree (cum laude) in electronic engineering, the Ph.D. degree in applied electromagnetics, and the Laurea degree (cum laude) in physics from the ''La Sapienza'' University of Rome, Rome, Italy, in 1986, 1991, and 1995, respectively. Upon his graduation in electronic engineering, he joined Italian Energy and Environment Agency (ENEA), where he was initially involved with free electron generators of millimeter waves and then on microwave components and antennas for heating of thermonuclear plasmas. In 1992, he joined as a Researcher of electromagnetics with the ''La Sapienza'' University of Rome. In 1998, he joined the Department of Engineering, Section of Applied Electronics, ''Roma Tre'' University, Rome, where he was an Associate Professor, from 1998 to 2005, and has been a Full Professor of electromagnetic fields, since 2005. From 2013 to 2017, he was the Deputy Director for Research with the Department of Engineering. From 2017 to 2022, he was with Roma Tre University as a Rector's Delegate for North America technology transfer. He is currently with the Department of Industrial, Electronic, and Mechanical Engineering. His research interests include structures for guiding and radiation of electromagnetic fields for microwave and millimeter waves applications, scattering, diffractive optics, plasma heating and current drive, electromagnetic band gap (EBG) media, and anisotropic media. He is a member of several scientific and technical societies in the frame of information technology, in particular in the field of electromagnetic systems. He is a member of the editorial boards and technical program committees of several international journals and conferences in the field of microwaves and antennas. He is an Associate Editor of IEEE OPEN JOURNAL OF ANTENNAS AND PROPAGATION.

Open Access funding provided by 'Università degli Studi Roma Tre' within the CRUI CARE Agreement